FULL PAPER

WILEY

Graphene-induced planarization of cyclooctatetraene derivatives

Asja A. Kroeger [ORCID] | Amir Karton [ORCID]

School of Molecular Sciences, The University of Western Australia, Perth, Australia

Correspondence
Amir Karton, School of Molecular Sciences, The University of Western Australia, Perth, WA 6009, Australia.
Email: amir.karton@uwa.edu.au

Funding information
Australian Research Council, Grant/Award Number: FT170100373

[Correction added on 28 October 2021, after first online publication: ORCID ID added for first author]

Abstract

Stable equilibrium compounds containing a planar antiaromatic cyclooctatetraene (COT) ring are promising candidates for organic electronic devices such as organic semiconductor transistors. The planarization of COT by incorporation into rigid planar π-systems, as well as by oxidation or reduction has attracted considerable attention in recent years. Using dispersion-corrected density functional theory calculations, we explore an alternative approach of planarizing COT derivatives by adsorption onto graphene. We show that strong π–π stacking interactions between graphene and COT derivatives induce a planar structure with an antiaromatic central COT ring. In addition to being reversible, this strategy provides a novel approach for planarizing COT without the need for incorporation into a rigid structure, atomic substitution, oxidation, or reduction.

KEYWORDS
density functional theory, dispersion interactions, planar cyclooctatetraene, π–π interactions

1 | INTRODUCTION

1,3,5,7-Cyclooctatetraene (COT, Figure 1) is the smallest $4n$ π-electron cyclic polyene with alternating single and double bonds that adopts a tub-shaped equilibrium structure. The nonplanar D_{2d} symmetric COT structure can undergo a dynamic tub-to-tub inversion via a planar bond-alternating D_{4h} symmetric transition structure (TS) (Figure 1).[1,2,3] It is well established that the tub-shaped equilibrium structure is nonaromatic while the planar TS of the ring inversion is antiaromatic.[4,5]

There has been considerable interest over the past two decades in constraining derivatives of COT to adopt a planar equilibrium structure.[1,4,6,7] Due to the antiaromaticity of the planar COT ring, the resulting compounds have unique electronic properties such as tuneable HOMO/LUMO levels, making them promising candidates for efficient organic semiconductors.[8,9,10] It has been demonstrated both experimentally and computationally that COT can be planarized through annulation with strained rings or by incorporation into a rigid planar π-system, forcing the central COT moiety to adopt a planar geometry with alternating single and double bonds.[1,4,8,9,11–24] Merino and coworkers showed that an alternative approach for planarizing COT to

adopt a D_{4h} symmetric structure is substitution of four alternating carbons with heavier group 14 elements (Si, Ge, and Sn).[25] Based on statistical analysis of X-ray data of 47 COT rings, Dominikowska and Palusiak further found that COT planarizes when acting as an effective π-type ligand in various organometallic complexes.[26] They also showed that aromatization of COT due to charge transfer from the metal to the ring (i.e., conversion from a $4n$ to a $4n + 2$ π-system, COT → COT^{2-}) is not a major factor in this planarization process. In this context, we note that another approach for planarizing COT is oxidation or reduction.[27–33] While this planarization approach has more typically employed metal ions, recently, Cohen and co-workers studied the nanomechanical response of COT to application of an external gate voltage on a graphene device, predicting planarization upon electron- and hole-doping.[31] Closer to the context of the present work, it was further recently found that COT-derived π-extended diaza[8]circulenes planarize on a gold surface.[34] Further, an acene-fused COT-derived mechaophore was recently reported to adopt a near-planar geometry in the crystalline phase due to thermal void collapse.[35]

In the present contribution, we explore an alternative approach for reversibly planarizing neutral COT derivatives via noncovalent π–π interactions with graphene. We use dispersion-corrected density
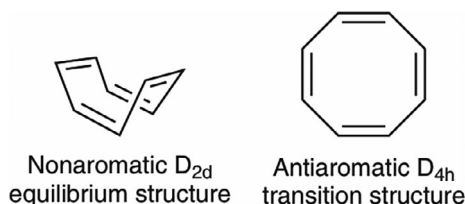
FIGURE 1 Schematic representation of the tub-shaped equilibrium structure of 1,3,5,7-cyclooctatetraene (COT) and the planar TS of its tub-to-tub ring inversion. TS, transition structure
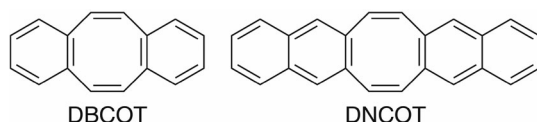

FIGURE 2 Schematic representation of the structures of dibenzo [a,e]cyclooctatetraene (DBCOT) and dinaphtho[a,e]cyclooctatetraene (DNCOT). For clarity the structures are shown as planar, although the equilibrium structures are strongly tub-shaped

functional theory (DFT) calculations to show that upon adsorption onto graphene dibenzo[a,e]cyclooctatetraene (DBCOT, Figure 2) can adopt a planar equilibrium structure. Likewise, dinaphtho[a,e] cyclooctatetraene (DNCOT, Figure 2) planarizes when adsorbed on graphene. In both cases, the central COT ring is converted from non-aromatic (in free v-shaped DBCOT and DNCOT) to antiaromatic upon adsorption on graphene. These results demonstrate that substantial $\pi-\pi$ interactions between graphene and DBCOT or DNCOT can induce planarity in the central COT ring. Thus, this provides a novel approach for reversibly planarizing COT without the need for a rigid network of substituents, atomic substitution, oxidation, or reduction. These results are consistent with previous works, which showed that multiple $\pi-\pi$ interactions can collectively provide significant energetic stabilization.[36-44] In this context, ref. 44 is of particular relevance since it demonstrates that a graphene sheet can catalyze the tub-to-tub inversion in COT and its ortho- and meta-benzannulated derivatives. Here we show that para benzannulated COT derivatives (e.g., DBCOT and DNCOT) form planar local minima on a graphene sheet.

2 | COMPUTATIONAL DETAILS

The geometries of all structures were fully optimized without constraints at the B3LYP-D3(BJ)/Def2-SVP level of theory,[45-48] where empirical D3 dispersion corrections[49] are included using the Becke–Johnson[50] damping potential (denoted by the suffix D3[BJ]). We note that B3LYP-D3(BJ) was found to give accurate geometries for both equilibrium and TSs of a wide range of organic and inorganic systems.[51,52,53,54,55] Harmonic vibrational frequencies were obtained at the same level of theory. The equilibrium structures were verified to

have all-real harmonic frequencies and the TSs to have only one imaginary frequency, which corresponds to the expected motion along the reaction coordinate. The connectivities of the transition and equilibrium structures were confirmed via intrinsic reaction coordinate (IRC) calculations[56] at the B3LYP-D3(BJ)/Def2-SVP level of theory. In order to obtain accurate binding energies and reaction barrier heights single point energy calculations were carried out using the hybrid meta-GGA (generalized gradient approximation) DFT method PW6B95 in conjunction with the large quadruple-ζ Def2-QZVP basis set.[57] For the single-point energy (SPE) calculations, we consider the D3(BJ) dispersion correction as well as the more recently developed, atomic-charge dependent D4 dispersion correction.[58,59] We note that the empirical D4 dispersion term accounts for 86%–88% of the interaction energies ($\Delta E_{e,int}$) in the DBCOT@$C_{96}H_{24}$ and DNCOT@$C_{96}H_{24}$ complexes. The PW6B95 exchange-correlation functional has been extensively benchmarked and found to be robust for both reaction energies and barrier heights involving related systems.[42,44,60-67] All geometry optimizations, frequency, and SPE calculations were carried out using the Gaussian 16 program suite.[68]

Nucleus independent chemical shift (NICS)[69,70] scans were performed by means of the gauge independent atomic orbitals (GIAO) method at the GIAO-B3LYP/6-311+G(d,p) level of theory with the Aroma 1.0 package.[5,71-73] This method involves placing the NICS probes at the geometric center of the aromatic or antiaromatic ring and scanning along the perpendicular z axis from 0.0 to 3.9 Å at intervals of 0.1 Å. The reported shielding tensor elements are the out-of-plane zz-components ($NICS_{ZZ}$). We note that $NICS(r)_{ZZ}$ denotes the $NICS_{ZZ}$ value at a distance of r Å above the molecular plane. In scans involving a planar COT derivative adsorbed onto a planar graphene nanoflake, the NICS scan above the substrate is directed away from the graphene nanoflake. In addition, the effect of the graphene flake on the $NICS_{ZZ}$ values has been backtracked by performing a $NICS_{ZZ}$ scan with the substrate removed. In order to visualize the ring currents in the planar COT, DBCOT, and DNCOT rings we performed anisotropy of the induced current density (AICD) analysis at the B3LYP/6-31G(d) level of theory,[74,75] where the magnetic field is set as orthogonal to the planes of the rings, and isosurfaces are plotted using an isosurface value of 0.025.

To gain further insights into the nature of the noncovalent interactions between the COT derivatives of interest and the graphene nanoflake, a second-generation energy decomposition analysis (EDA)[76] based on absolutely localized molecular orbitals (ALMOs) was performed in conjunction with the Def2-SVP basis set. The EDA calculations were carried out with the ωB97M-V exchange correlation functional[77] as recommended in ref. 76. These calculations were carried out with the Q-Chem 5.2 program suite.[78] Overlays of structures and root-mean-square deviations (RMSDs) of atomic positions between structures were obtained using Mercury.[79] All remaining 3D structural representations were generated using CYLview.[80]

3 | RESULTS AND DISCUSSION

3.1 | Ring inversion in isolated COT, DBCOT, and DNCOT

To examine the free planar structures of interest, we begin by examining the tub-to-tub inversion process in free COT, DBCOT, and DNCOT. Figure 3 shows the tub-shaped equilibrium structures and the planar ring-inversion TSs. The COT equilibrium structure adopts a tub-shaped geometry of D_{2d} symmetry with alternating single and double bonds of 1.473 and 1.344 Å, respectively. These bond lengths are in excellent agreement with the experimental values of 1.4702

± 0.0005 and 1.3371 ± 0.001 Å obtained from femtosecond time-resolved rotational coherence spectroscopy and ab initio calculations.[81] The calculated dihedral angle between vicinal double bonds of 54.2° is in good agreement with the experimental value of 56° obtained from low temperature X-ray analysis.[82,83] The planar TS for the tub-inversion lies 58.4 kJ mol^{-1} above the equilibrium structure on the Gibbs free energy surface at the PW6B95-D4/Def2-QZVP level of theory. Using the high-level composite ab initio W1-F12 protocol[84] we obtain $\Delta G^{\ddagger}_{298} = 58.7$ kJ mol^{-1} at the CCSD(T)/CBS level of theory (coupled cluster energy with single, double, and quasiperturbative triple excitations close to the complete basis-set limit).[85] The good agreement with W1-F12 theory increases our

(A)

COT 58.4 kJ mol^{-1}

DBCOT 52.3 kJ mol^{-1}

DNCOT 41.0 kJ mol^{-1}

(B)

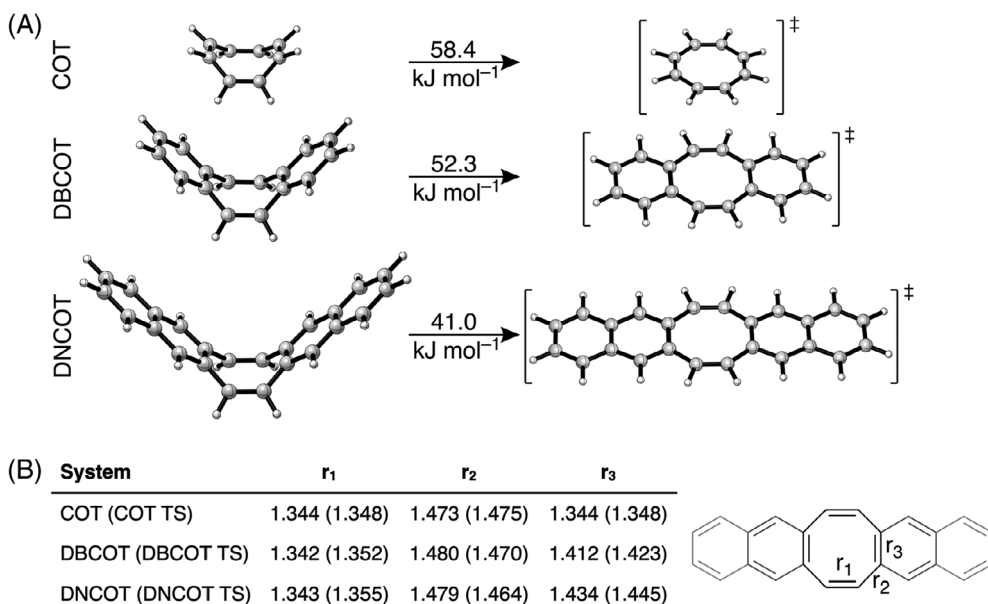| System	r_1	r_2	r_3
COT (COT TS)	1.344 (1.348)	1.473 (1.475)	1.344 (1.348)
DBCOT (DBCOT TS)	1.342 (1.352)	1.480 (1.470)	1.412 (1.423)
DNCOT (DNCOT TS)	1.343 (1.355)	1.479 (1.464)	1.434 (1.445)

FIGURE 3 Optimized structures of the tub-shaped equilibrium structures and ring-inversion TSs for cyclooctatetraene (COT), dibenzo[a,e]cyclooctatetraene (DBCOT), and dinaphtho[a,e] cyclooctatetraene (DNCOT). Selected bond distances are given in Å and PW6B95-D4/Def2-QZVP Gibbs free energies of activation are given in kJ mol^{-1}. TS, transition structure
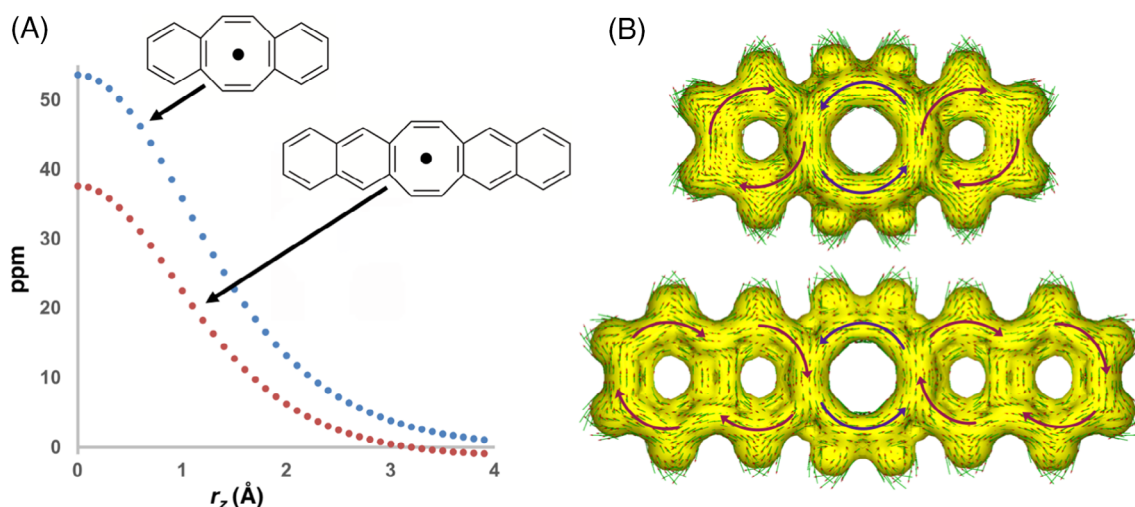

FIGURE 4 (A) NICS$_{ZZ}$ scans at heights of 0.0–3.9 Å above the molecular plane of the inversion TSs of DBCOT and DNCOT (the NICS$_{ZZ}$ scan for unsubstituted COT results in NICS(0)$_{ZZ}$ = 133.6 and NICS(1)$_{ZZ}$ = 103.3 ppm and is not shown here for the sake of clarity) and (B) AICD plots of the induced ring currents in the planar DBCOT and DNCOT, with paratropic (counter-clockwise) ring currents indicated by blue arrows and diatropic (clockwise) ring currents indicated by red arrows. AICD, anisotropy of the induced current density; COT, cyclooctatetraene; DBCOT, dibenzo[a,e]cyclooctatetraene; DNCOT, dinaphtho[a,e]cyclooctatetraene

—WILEY

confidence in the PW6B95-D4/Def2-QZVP level of theory. Para dibenzannulation of COT (to form DBCOT) results in little change in the lengths of the unsubstituted single and double bonds, but as expected, the length of the substituted double bonds increases from 1.344 Å (in COT) to 1.412 Å (in DBCOT). A similar elongation of the substituted double bonds is observed in the planar TS, namely the bond lengths increase from 1.348 Å (in COT) to 1.423 Å (in DBCOT). Further para dibenzannulation of DBCOT (to form DNCOT) results in little change of bond lengths and angles of the central COT ring (Figure 3).

While there are few structural changes in the central COT moiety upon going from DBCOT to DNCOT, Figure 3 shows that with increasing annulation, inversion barrier heights are reduced in the following order: $\Delta G^{\ddagger}_{298} = 58.4$ (COT), 52.3 (DBCOT), and 41.0 (DNCOT) kJ mol^{-1}. As the antiaromaticity of planar COT has been of significant interest, we performed NICS$_{ZZ}$ scans above the central COT moiety of the planar parent compound, DBCOT and DNCOT. These results are displayed in Figure 4. The antiaromaticity of the central COT ring in the TS is systematically reduced with the degree of benzannulation. For example, the NICS(1)$_{ZZ}$ values (in ppm) are 103.3 (COT), 35.8 (DBCOT), and 22.5 (DNCOT). As antiaromatic compounds are known to typically be unstable, the observed reduction in inversion barriers with increasing annulation may thus in part be associated with the decreased antiaromaticity of the central COT moiety in the same order. In order to gain more detailed insights into the global and semi-global ring-currents in the systems of interest, we use the AICD method to visualize the ring currents in the planar DBCOT and DNCOT systems (Figure 4). In agreement with the NICS$_{ZZ}$ analysis we find that the planar COT exhibits a strong paratropic ring current, confirming its antiaromaticity (Figure S1). In the benzo- and naptho-fused DBCOT and DNCOT, the central COT moiety still displays distinct paratropicity (and hence antiaromaticity) but directly encounters the diatropic ring currents of the neighboring benzo- and naptho-units, explaining the reduced antiaromaticity of the central COT moiety captured by the NICS(1)zz values. Similar observations were previously made for a dibenzannulated indacene derivative, where benzannulation reduced the paratropicity of the antiaromatic indacene unit.[86] We note that the AICD plot for DNCOT further captures the distinct semi-global diatropic ring current of the [10]annulene peripheries of the naphtho-moieties.[75] Finally, we note that since these are multi-ring systems it is important to perform NICS scans in the XY-plane across all the benzene and COT rings.[5,73,87] Consistent with the AICD results, these scans show negative NICS values for the benzo/naphto-rings and positive NICS values for the central COT ring with a maximum at its geometric center (see Figure S2 of the Supporting Information).

3.2 | Structure of DBCOT adsorbed on a graphene nanoflake

We recently found that adsorption of COT onto a graphene nanoflake catalyst (C$_{96}$H$_{24}$) reduces its ring inversion barrier height by 20% of the uncatalyzed reaction barrier height.[44] Structural and energetic analyses show that this catalytic activity is driven by shape complementarity between the planar 2D catalyst and planar TS. Namely, the 2D nanomaterial stabilizes the planar TS to a greater extent than the highly nonplanar, tub-shaped reactant. It is important to emphasize that both the free and adsorbed planar COT structures are first-order saddle points possessing an imaginary frequency that corresponds to the tub-inversion.[44]

In contrast, in the current work we find that the planar structure of para dibenzannulated COT adsorbed on graphene is no longer a first-order saddle point, but a local minimum with all-real frequencies (the optimized structure of the equilibrium complex is depicted in Figure 5). Thus, it seems that in the case of DBCOT, the graphene monolayer reshapes the PES such that the TS for the tub-inversion becomes a local minimum.[88] As mentioned above, when the graphene catalyst is removed, we obtain a planar TS for the DBCOT tub-inversion possessing an imaginary frequency of 50.1i cm^{-1} (Figure 3). To double check that the planar DBCOT adsorbed on graphene (Figure 5A) is an equilibrium structure and not a TS, we also optimize this structure using an inherently different DFT functional than B3LYP-D3(BJ), namely the M06-2X functional.[89,90] M06-2X is a hybrid-meta GGA functional which includes a significantly higher percentage of exact exchange compared to B3LYP (i.e., 54% vs. 20%, respectively). Another key difference between B3LYP-D3(BJ) and M06-2X is that the latter is more heavily parametrized and incorporates dispersion interactions into the parametrization of the functional, rather than via a molecular mechanics-type correction that is used in B3LYP-D3(BJ). The M06-2X/Def2-SVP optimized planar para dibenzannulated COT structure adsorbed on graphene is a local minimum with all-real frequencies, very similar to the B3LYP-D3 (BJ) structure (see the Supporting Information for the optimized structure of the equilibrium complex).

Next we compare the structure of the planar equilibrium DBCOT adsorbed on graphene (Figure 5A) with that of the planar ring-inversion TS (Figure 3). For the sake of brevity, the planar DBCOT equilibrium complex (Figure 5a) will be denoted as DBCOT$_{planar}$@C$_{96}$H$_{24}$. Inspection of the bond distances in Figures 3 and 5 reveals a remarkable similarity between the planar equilibrium and first-order saddle point DBCOT structures. The bond lengths of the ring-inversion TS are practically unchanged upon adsorption on the graphene nanoflake—namely, with changes in bond lengths of less than 0.001 Å upon adsorption. Overall, the RMSD of the atomic positions between the free inversion TS and adsorbed equilibrium structure is 0.015 Å (for further details see Table S1 of the Supporting Information). On the electronic PES, the energy difference between the fully optimized free TS and planar DBCOT in the geometry it adopts in the complex is merely ΔE_e = 0.26 kJ mol^{-1} at the PW6B95-D4/Def2-QZVP level of theory. This negligibly small energetic difference between the free TS and adsorbed planar equilibrium DBCOT structure, along with the remarkable similarity between their structures, indicate that the presence of the graphene flake indeed converts the free planar DBCOT TS into a minimum on the PES.
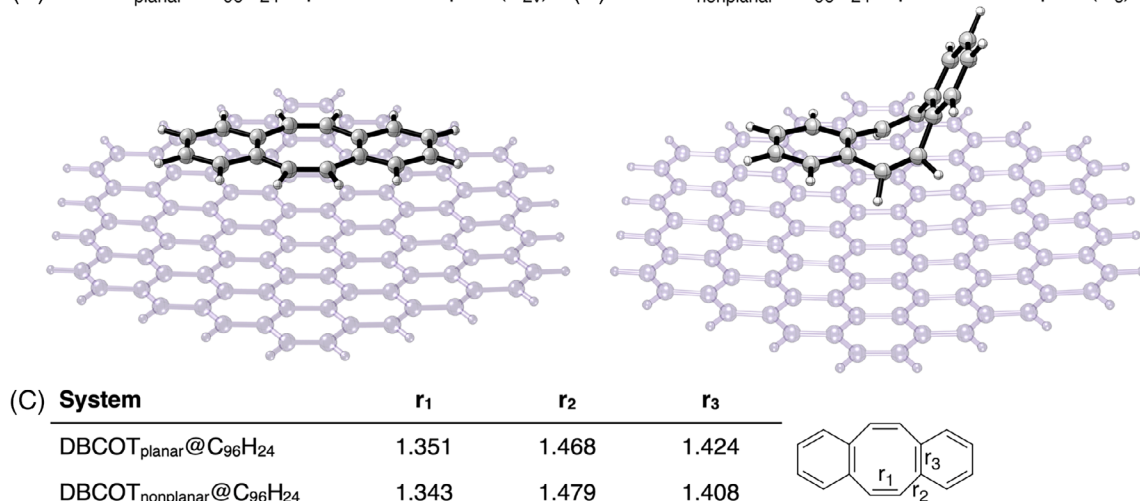
FIGURE 5 Optimized structures of the (A) planar DBCOT@C$_{96}$H$_{24}$ equilibrium complex (C$_{2v}$ symmetry), (B) nonplanar DBCOT@C$_{96}$H$_{24}$ equilibrium complex (C$_s$ symmetry), and (C) selected bond distances in Å. DBCOT, dibenzo[a,e]cyclooctatetraene

It is well established that external interactions can reshape a PES in a way that critical points are created or eliminated. A textbook example is the Menshutkin S$_N$2 reaction, where strong solvation effects convert a single-well PES into a double-well PES.[91] The gas-phase PES for this reaction has also been found to be modified in the presence of various nanotubes and surfaces (including a graphene monolayer).[92,93,94,95,96] Another example where external effects dramatically affect critical points on a PES, is the intramolecular chlorine transfer in chlorinated carnosine which is coupled with two sequential intramolecular proton shifts.[97] In the gas-phase these three atom transfers occur in a concerted TS; however in aqueous solution they proceed via three separate TSs. Another example where a TS becomes a stable minimum on the PES, is provided by the recent work of Solel et al.,[98] which showed that steric repulsion in a substituted corannulene derivative converts planar corannulene, which would normally be a TS on the PES, into an experimentally isolable equilibrium structure. Finally, it should be mentioned that external influences (e.g., coordination, oxidation, reduction, and chemical substitution) have been shown to play a role in structure manipulation of planar and quasi planar systems due to their effect on vibronic pseudo Jahn–Teller couplings.[99,100,101,102,103]

Here, we postulate that reshaping of the PES may arise if the interaction energy between the graphene and the planar DBCOT is larger than the reaction barrier height for the tub-inversion in free DBCOT. Table 1 gives the interaction energies between the C$_{96}$H$_{24}$ flake and DBCOT. On the electronic PES, the interaction energy between C$_{96}$H$_{24}$ and DBCOT amounts to 99.1 kJ mol^{-1} while the reaction barrier height for the tub-inversion in free DBCOT is just 40.8 kJ mol^{-1}. We note that here, the interaction energy is calculated as the energy difference between the fully optimized DBCOT$_{planar}$@C$_{96}$H$_{24}$ complex and isolated monomers in their geometry in the complex. However, it should be noted that separating the optimized DBCOT$_{planar}$@C$_{96}$H$_{24}$ complex into the

TABLE 1 Stabilization and interaction energies in the equilibrium complexes formed between graphene nanoflake (C$_{96}$H$_{24}$) and the DBCOT and DNCOT substrates calculated on the electronic (ΔE_e) and Gibbs free (ΔG_{298}) PESs (PW6B95-D4/Def2-QZVP, kJ mol^{-1})

Equilibrium complex	$\Delta E_{e,int}$[a]	$\Delta E_{e,stab}$[b]	$\Delta G_{298,stab}$[b]
DBCOT$_{nonplanar}$@C$_{96}$H$_{24}$	65.4	59.3	8.6
DBCOT$_{planar}$@C$_{96}$H$_{24}$	99.1	97.4	45.7
DNCOT$_{planar}$@C$_{96}$H$_{24}$	139.7	139.1	76.1

Abbreviations: DBCOT, dibenzo[a,e]cyclooctatetraene; DNCOT, dinaphtho[a,e]cyclooctatetraene.
[a]Interaction energies taken as the difference between the fully optimized complex and isolated monomers in their geometry in the complex.
[b]Stabilization energies taken as the difference between the fully optimized complex and isolated monomers in the following way: DBCOT$_{nonplanar}$@C$_{96}$H$_{24}$ → DBCOT$_{nonplanar}$ + C$_{96}$H$_{24}$; DBCOT$_{planar}$@C$_{96}$H$_{24}$ → DBCOT$_{planar}$(TS) + C$_{96}$H$_{24}$; DNCOT$_{planar}$@C$_{96}$H$_{24}$ → DNCOT$_{planar}$(TS) + C$_{96}$H$_{24}$ (see text).

free optimized tub-inversion TS and C$_{96}$H$_{24}$ graphene flake (i.e., DBCOT$_{planar}$@C$_{96}$H$_{24}$ → DBCOT$_{planar}$(TS) + C$_{96}$H$_{24}$) has a very similar energetic cost of 97.4 kJ mol^{-1} (Table 1). This separation provides an estimation for the energetic stabilization provided by the C$_{96}$H$_{24}$ flake to the inversion TS. Thus, it is clear that the energetic stabilization provided by the C$_{96}$H$_{24}$ flake is much larger than the barrier height for the tub-inversion. Due to entropic effects this energy difference becomes smaller on the Gibbs free PES at 298 K. Namely, the reaction barrier height for the inversion of free DBCOT is $\Delta G^{\ddagger}_{298}$ = 52.3 kJ mol^{-1} (Figure 3), and the energetic stabilization provided by the C$_{96}$H$_{24}$ graphene flake to the TS amounts to 45.7 kJ mol^{-1} (Table 1).

In the above-mentioned DBCOT$_{planar}$@C$_{96}$H$_{24}$ complex (Figure 5A) both benzene rings are parallel to the graphene monolayer, resulting in a planar antiaromatic COT ring. However, the nonaromatic, tub-shaped DBCOT structure can also adsorb on
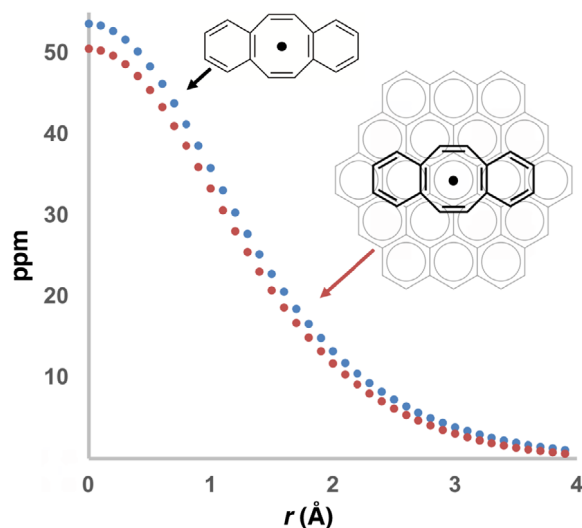
FIGURE 6 $NICS_{ZZ}$ scans at heights of 0.0–3.9 Å above the molecular plane of the inversion TS in free DBCOT and the equilibrium planar DBCOT$_{planar}$@C$_{54}$H$_{18}$ complex. The vertical distance between the geometric centers of the COT and central benzene ring of the graphene flake is 3.27 Å. DBCOT, dibenzo[a,e]cyclooctatetraene; TS, transition structure

graphene such that only one benzene ring is parallel to the graphene sheet (DBCOT$_{nonplanar}$@C$_{96}$H$_{24}$, Figure 5B). Thus, the planarization process of DBCOT on graphene (DBCOT$_{nonplanar}$@C$_{96}$H$_{24}$ → DBCOT$_{planar}$@C$_{96}$H$_{24}$) is a measure of the energetic trade-off between the stronger noncovalent interactions in DBCOT$_{planar}$@C$_{96}$H$_{24}$ and the net planarization energy of the central COT ring. At the PW6B95-D4/Def2-QZVP level of theory, DBCOT$_{nonplanar}$@C$_{96}$H$_{24}$ is more stable than DBCOT$_{planar}$@C$_{96}$H$_{24}$ by 2.7 kJ mol^{-1} on the electronic PES and 15.2 kJ mol^{-1} on the Gibbs free PES. These energies should be compared to the planarization barrier heights in the gas-phase, namely $\Delta E_e = 40.8$ and $\Delta G_{298} = 52.3$ kJ mol^{-1} (Figure 3). Thus, the graphene sheet reduces the net planarization energy by ca. 38.0 kJ mol^{-1}. These results suggest that the molecular shape and antiaromatic/nonaromatic character of DBCOT could be easily modulated on a graphene surface.

We have shown above that the planar DBCOT interacts strongly with the C$_{96}$H$_{24}$ flake in the DBCOT$_{planar}$@C$_{96}$H$_{24}$ complex, which forms a minimum on the PES. Thus, it is instructive to examine whether the interaction with the graphene flake affects the antiaromaticity of DBCOT relative to that of the free DBCOT TS. Figure 6 plots the $NICS_{ZZ}$ scans above the central COT ring in the DBCOT inversion TS and the equilibrium DBCOT$_{planar}$@C$_{54}$H$_{18}$ complex. For reasons of computational cost, the $NICS_{ZZ}$ scans were conducted on DBCOT$_{planar}$@C$_{54}$H$_{18}$ rather than the much larger DBCOT$_{planar}$@C$_{96}$H$_{24}$ complex. The $NICS_{ZZ}$ scans show that the antiaromatic character of the DBCOT remains practically unchanged by the interaction with the graphene flake. For example, the $NICS(1)_{ZZ}$ values (in ppm) are 35.8 (free DBCOT TS) and 33.3 (DBCOT$_{planar}$@C$_{54}$H$_{18}$).

3.3 | Structure of DNCOT adsorbed on a graphene nanoflake

In the previous section we have seen that strong interactions between graphene and DBCOT give rise to a planar antiaromatic DBCOT equilibrium structure in the DBCOT$_{planar}$@C$_{96}$H$_{24}$ complex. However, the equilibrium complex in which the DBCOT monomer is nonplanar and nonaromatic (DBCOT$_{nonplanar}$@C$_{96}$H$_{24}$) was found to be more stable by 15.2 kJ mol^{-1} on the ΔG_{298} energy surface. A natural question is what happens upon further para dibenzannulation of DBCOT to form DNCOT (Figure 3). In this case, we were only able to locate the equilibrium complex (with all-real harmonic frequencies) in which DNCOT adsorbed on graphene is planar (DNCOT$_{planar}$@C$_{96}$H$_{24}$, Figure 7).[88] Similar to the case of DBCOT$_{planar}$@C$_{96}$H$_{24}$ above, we also optimized the DNCOT$_{planar}$@C$_{96}$H$_{24}$ structure at the M06-2X/Def2-SVP level of theory and confirmed it is a local minimum with all-real frequencies (for the optimized structure see the Supporting Information). The bond distances in Figures 3 and 5 demonstrate that the planar equilibrium DNCOT adsorbed on graphene and the first-order saddle point DNCOT structures are similar. Namely, the bond lengths in the ring-inversion TS are changed by less than 0.001 Å upon adsorption on the graphene nanoflake. Overall, the RMSD of atomic positions between the free inversion TS and adsorbed equilibrium structure is 0.034 Å (for further details see Table S1 of the Supporting Information). On the electronic PES, the energy difference between the free planar TS and the planar geometry of the equilibrium complex is $\Delta E_e = 1.4$ kJ mol^{-1} at the PW6B95-D4/Def2-QZVP level of theory. Thus, similar to the case of DBCOT the small energetic difference between the free inversion TS and adsorbed equilibrium DNCOT structure, along with their structural similarity, indicates that adsorption onto the graphene flake converts the free planar DNCOT TS into a minimum on the PES. As expected, the electronic interaction energy between the graphene flake and DNCOT in the DNCOT$_{planar}$@C$_{96}$H$_{24}$ complex (139.7 kJ mol^{-1}) is substantially larger than that between the graphene flake and the smaller DBCOT (99.1 kJ mol^{-1}, Table 1). Similarly, on the ΔG_{298} energy surface, the energetic stabilization provided by the C$_{96}$H$_{24}$ flake to the planar conformer is 45.7 (DBCOT$_{planar}$@C$_{96}$H$_{24}$) and 76.1 (DNCOT$_{planar}$@C$_{96}$H$_{24}$) kJ mol^{-1}. When comparing the latter Gibbs-free stabilization energy to the Gibbs free-activation energy required to planarize the free DNCOT ($\Delta G^{\ddagger}_{298} = 41.0$ kJ mol^{-1}, Figure 3) it is clear that the energetic stabilization provided by the C$_{96}$H$_{24}$ flake is substantially larger than the barrier height for the tub-inversion in DNCOT.

Removing one naphto-group from DNCOT results in NCOT. For NCOT we were able to optimize complexes between both the planar and nonplanar conformers and the graphene sheet. For the planarization process of NCOT on graphene (i.e., NCOT$_{nonplanar}$@C$_{96}$H$_{24}$ → NCOT$_{planar}$@C$_{96}$H$_{24}$) we obtain reaction energies of $\Delta E_e = 3.3$ and $\Delta G_{298} = 11.4$ kJ mol^{-1} at the PW6B95-D4/Def2-QZVP level of theory. These reaction energies are similar to those obtained for DBCOT@C$_{96}$H$_{24}$ (vide supra).

(A) DNCOT$_{planar}$@C$_{96}$H$_{24}$ equilibrium complex (C$_{2v}$)

(B)

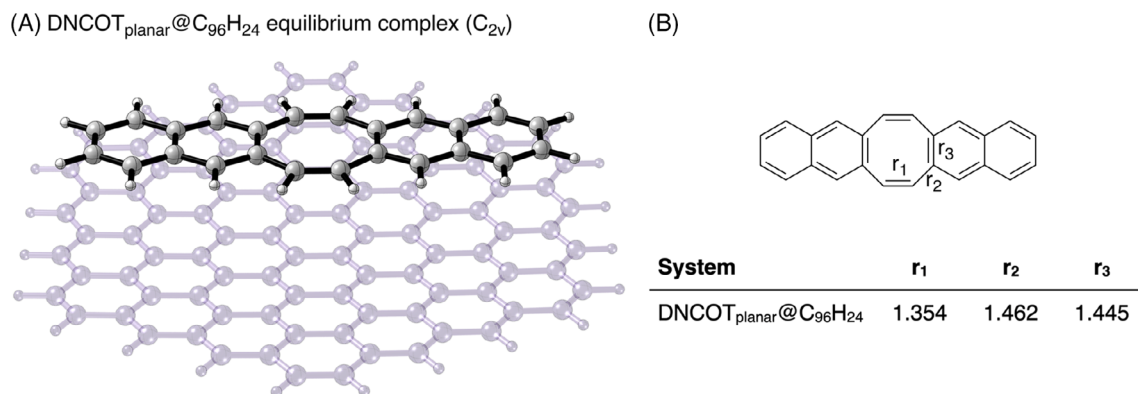| System	r$_1$	r$_2$	r$_3$
DNCOT$_{planar}$@C$_{96}$H$_{24}$	1.354	1.462	1.445

FIGURE 7 (A) Optimized structure of the planar DNCOT@C$_{96}$H$_{24}$ equilibrium complex and (B) selected bond distances in Å. DNCOT, dinaphtho[a,e]cyclooctatetraene
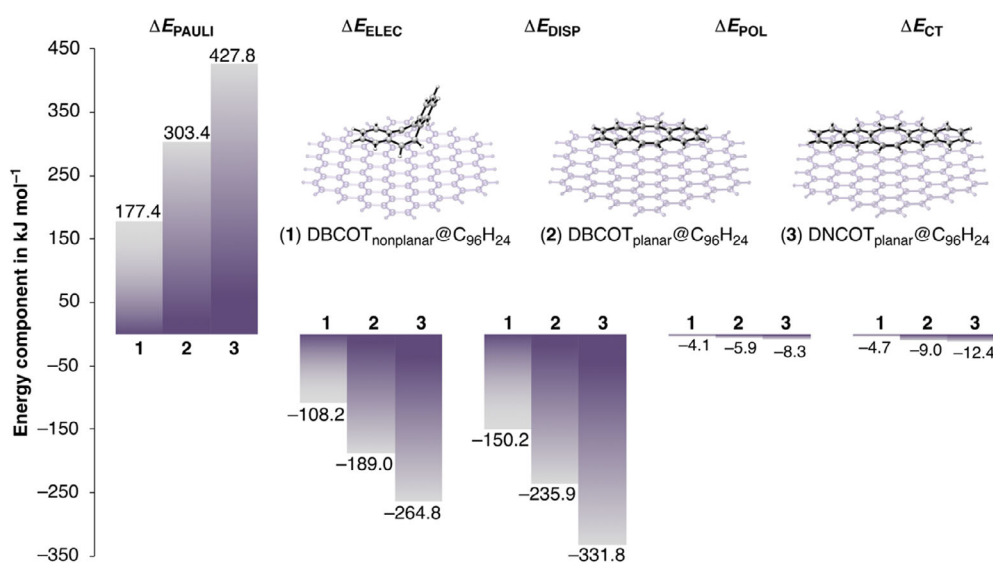

FIGURE 8 Breakdowns of the intermolecular interaction energies between the graphene flake and the planar and nonplanar COT derivatives of interest obtained from second generation ALMO-EDA at the ωB97M-V/Def2-SVP level of theory. COT, cyclooctatetraene

3.4 | Noncovalent interactions responsible for the stabilization of the adsorbed COT derivatives

In order to gain more detailed insights into the energy components contributing to the above noncovalent stabilization energies we performed energy decomposition analyses using the second-generation ALMO-EDA scheme by Head-Gordon and co-workers.[76] These analyses allow us to obtain measures of the contributions of Pauli repulsion (ΔE_{PAULI}), electrostatic interactions (ΔE_{ELEC}), dispersion interactions (ΔE_{DISP}), as well as polarization (ΔE_{POL}) and charge transfer (ΔE_{CT}) to overall intermolecular interaction energies. Figure 8 gives the resulting breakdowns of the intermolecular interaction energies between the graphene flake and the COT derivatives of interest in the planar and nonplanar conformations.

As apparent from inspection of Figure 8, the magnitudes of all energy terms are smallest in the complex between the flake and the nonplanar DBCOT conformer, which is adsorbed onto the flake through only one benzene ring. These magnitudes increase with increasing numbers of aromatic rings interacting with the flake in the

complexes with the planar conformers of DBCOT and the larger DNCOT. Hereby, there are clear trends in the contributions of the individual energy terms to overall interaction energies. Contributions from both charge transfer (representing donor–acceptor orbital interactions between flake and substrate) as well as polarization (interaction energies resulting from induced electrostatic interactions in response to the other monomer in the complex) are small, largely remaining below 10 kJ mol^{-1}. On the other hand, the largest destabilizing contributions to overall interaction energies in all systems result from Pauli repulsions, which destabilize the complexes by amounts ranging between 177.4 and 427.8 kJ mol^{-1}. These large destabilizations are, however, in all cases outweighed by significant stabilizations from permanent electrostatic and dispersion interactions between flake and substrate. In particular, these stabilizing contributions together amount to 258.4, 424.9, and 596.6 kJ mol^{-1} in complexes **1**–**3**. When further comparing the individual contributions from electrostatic and dispersion interactions, we find that despite often being considered weak, stabilizations from dispersion interactions are consistently larger than those resulting from electrostatic interactions.

This difference increases with increasing substrate size. Whereas the contributions from dispersion interactions are larger by 41.9 and 46.0 kJ mol^{-1} in complexes **1** and **2** with the smaller DBCOT, they are larger by 66.9 kJ mol^{-1} than the electrostatic contribution in the complex with the larger DNCOT. This increasing importance of dispersion interactions to the large stabilization experienced by π–π stacked systems of increasing size has previously been reported.[104] Overall, the EDA results indicate that the observed planarizations of DBCOT and DNCOT on graphene are largely driven by dispersion interactions and, to a smaller extent, electrostatic interactions, which are more pronounced in the π–π stacked complexes with the planar conformers.

Finally, since COT is known to planarize upon oxidation or reduction,[27,30,31] it is instructive to additionally examine the amount of charge transferred between graphene and the planar substrates upon complexation. This can be done by summing the overall atomic polar tensor (APT) charges on the graphene flake and substrate.[105] We note that APT charges have been shown to give reliable molecular charge distributions.[106,107] For both DBCOT$_{planar}$@C$_{96}$H$_{24}$ and DNCOT$_{planar}$@C$_{96}$H$_{24}$ complexes a small amount of negative charge is transferred from the planar substrate to the graphene flake, namely amounts of 0.05 and 0.09 e, respectively. Thus, consistent with the above EDA results, charge transfer seems to only play a minor role in the planarization process.

4 | CONCLUSIONS

There has been considerable interest in constraining derivatives of COT to adopt a planar equilibrium structure with antiaromatic character. It has been demonstrated experimentally and/or computationally that this can be achieved via annulation of COT with strained rings or by incorporation into a rigid planar π-system, atomic substitution, complexation with transition metals, oxidation, or reduction. Here, we propose an alternative approach for the reversible planarization of COT derivatives: We show that substantial π–π stacking interactions between arene-fused COT derivatives and graphene allow for these typically v-shaped derivatives to adopt a planar antiaromatic equilibrium structure in the complex. Thus, the external effect of the graphene flake appears to reshape the PES in a way to allow for TSs to become stable minima.

We postulate that this reshaping of the PES arises when the noncovalent interaction energies are larger than the planarization barriers. At the PW6B95-D4/Def2-QZVP level of theory we obtain stabilization energies by the graphene flake of 45.7 (DBCOT) and 76.1 (DNCOT) kJ mol^{-1} on the Gibbs free PES. The Gibbs free stabilization energy for DNCOT is much larger than the activation energy required to planarize the free compound and therefore DNCOT adopts a planar antiaromatic equilibrium structure on graphene. The Gibbs free stabilization energy for DBCOT is on par with the activation energy required to planarize the free DBCOT. Therefore, DBCOT can adsorb on graphene either as a planar antiaromatic or tub-shaped nonaromatic structure, both of which are equilibrium structures with all-real vibrational frequencies. The relatively small energy difference between these two complexes (2.7 kJ mol^{-1} on the electronic PES

and 15.2 kJ mol^{-1} on the Gibbs free PES) suggests that the molecular shape and antiaromatic/nonaromatic character of DBCOT could be modulated on a graphene surface.

The above results are further analyzed using NICS$_{ZZ}$ scans and energy decomposition analyses. NICS$_{ZZ}$ scans show that the central COT moiety in the planar DBCOT remains antiaromatic upon adsorbing on graphene. Energy decomposition analyses reveal that the strong interactions between the planar DBCOT/DNCOT and graphene are dominated by dispersion and electrostatic interactions, where the former is more pronounced in both cases. Overall, this study provides a novel approach for reversibly planarizing COT derivatives without the need for incorporation into a rigid π-system, atomic substitution, oxidation, or reduction.

DATA AVAILABILITY STATEMENT

The data that support the findings of this study are available in the supplementary material of this article and from the corresponding author upon reasonable request.

ORCID

Asja A. Kroeger https://orcid.org/0000-0001-7699-541X
Amir Karton https://orcid.org/0000-0002-7981-508X

REFERENCES

[1] T. Nishinaga, T. Ohmae, M. Iyoda, *Symmetry* **2010**, *2*, 76.
[2] J. I. Wu, I. Fernández, Y. Mo, P. v. R. Schleyer, *J. Chem. Theor. Comput* **2012**, *8*, 1280.
[3] A. Schild, B. Paulus, *J. Comput. Chem.* **2013**, *34*, 1393.
[4] F.-G. Klärner, *Angew. Chem., Int. Ed.* **2001**, *40*, 3977.
[5] A. Stanger, *Eur. J. Org. Chem.* **2020**, *2020*, 3120.
[6] E. L. Spitler, C. A. Johnson II., M. M. Haley, *Chem. Rev.* **2006**, *106*, 5344.
[7] T. M. Krygowski, H. Szatylowicz, O. A. Stasyuk, J. Dominikowska, M. Palusiak, *Chem. Rev.* **2014**, *114*, 6383.
[8] T. Ohmae, T. Nishinaga, M. Wu, M. Iyoda, *J. Am. Chem. Soc.* **2010**, *132*, 1066.
[9] T. Nishinaga, T. Ohmae, K. Aita, M. Takase, M. Iyoda, T. Arai, Y. Kunugi, *Chem. Commun.* **2013**, *49*, 5354.
[10] T. Nishinaga, *J. Syn. Org. Chem.* **2020**, *78*, 140.
[11] L. A. Paquette, T. Z. Wang, C. E. Cottrell, *J. Am. Chem. Soc.* **1987**, *109*, 3730.
[12] F. W. B. Einstein, A. C. Willis, *J. Chem. Soc., Chem. Commun.* **1981**, 526.
[13] K. K. Baldridge, J. S. Siegel, *J. Am. Chem. Soc.* **1992**, *114*, 9583.
[14] P. v. R. Schleyer, H. Jiao, H. M. Sulzbach, H. F. Schaefer, *J. Am. Chem. Soc* **1996**, *118*, 2093.
[15] A. Stanger, *J. Am. Chem. Soc.* **1998**, *120*, 12034.

[16] K. K. Baldridge, J. S. Siegel, *J. Am. Chem. Soc.* **2001**, *123*, 1755.

[17] A. Matsumura, K. Komatsu, *J. Am. Chem. Soc.* **2001**, *123*, 1768.

[18] Y. Nakamura, N. Aratani, H. Shinokubo, A. Takagi, T. Kawai, T. Matsumoto, Z. S. Yoon, D. Y. Kim, T. K. Ahn, D. Kim, A. Muranaka, N. Kobayashi, A. Osuka, *J. Am. Chem. Soc.* **2006**, *128*, 4119.

[19] Y. Nakamura, N. Aratani, A. Osuka, *Chem. – Asian J.* **2007**, *2*, 860.

[20] Y. Nakamura, N. Aratani, K. Furukawa, A. Osuka, *Tetrahedron* **2008**, *64*, 11433.

[21] T. Nishinaga, T. Uto, R. Inoue, A. Matsuura, N. Treitel, M. Rabinovitz, K. Komatsu, *Chem. Eur. J.* **2008**, *14*, 2067.

[22] J. R. Dias, J. Aihara, *Mol. Phys.* **2009**, *107*, 71.

[23] S. Bhowmik, M. Kosa, A. Mizrahi, N. Fridman, M. Saphier, A. Stanger, Z. Gross, *Inorg. Chem.* **2017**, *56*, 2287.

[24] T. Nishinaga, S. Shiroma, M. Hasegawa, *Org. Lett.* **2018**, *20*, 3426.

[25] G. Martinez-Guajardo, Z. Gomez-Saldoval, D. F. Jana, P. Calaminici, C. Corminboeuf, G. Merino, *Phys. Chem. Chem. Phys.* **2011**, *13*, 20615.

[26] J. Dominikowska, M. Palusiak, *New J. Chem.* **2010**, *34*, 1855.

[27] T. Bally, L. Truttmann, F. Williams, S. Dai, *J. Am. Chem. Soc.* **1995**, *117*, 7916.

[28] J. Dominikowska, M. Palusiak, *J. Comput. Chem.* **2011**, *32*, 1441.

[29] K. Mouri, S. Saito, S. Yamaguchi, *Angew. Chem., Int. Ed.* **2012**, *51*, 5971.

[30] A. Y. Sokolov, D. B. Magers, J. I. Wu, W. D. Allen, P. v. R. Schleyer, H. F. Schaefer, *J. Chem. Theory Comput.* **2013**, *9*, 4436.

[31] S. Oh, M. F. Crommie, M. L. Cohen, *ACS Nano* **2019**, *13*, 1713.

[32] H. Hamaoka, S. Shiroma, K. Aburaya, M. Hasegawa, T. Nishinaga, *ChemPlusChem* **2019**, *84*, 704.

[33] Y. Zhu, Z. Zhou, Z. Wei, M. A. Petrukhina, *Organometallics* **2020**, *39*, 4688.

[34] K. Nakamura, Q.-Q. Li, O. Krejčí, A. S. Foster, K. Sun, S. Kawai, S. Ito, *J. Am. Chem. Soc.* **2020**, *142*, 11363.

[35] T. Yamakado, K. Otsubo, A. Osuka, S. Saito, *J. Am. Chem. Soc.* **2018**, *140*, 6245.

[36] R. Podeszwa, *J. Chem. Phys.* **2010**, *132*, 44704.

[37] T. Janowski, A. R. Ford, P. Pulay, *Mol. Phys.* **2010**, *108*, 249.

[38] J. Bjork, F. Hanke, C. A. Palma, P. Samori, M. Cecchini, M. Persson, *J. Phys. Chem. Lett.* **2010**, *1*, 3407.

[39] S. Grimme, C. Mück-Lichtenfeld, J. Antony, *J. Phys. Chem. C* **2007**, *111*, 11199.

[40] A. Karton, *Chem. Phys. Lett.* **2014**, *614*, 156.

[41] P. A. Denis, *J. Phys. Chem. A* **2015**, *119*, 5770.

[42] A. A. Kroeger, A. Karton, *J. Org. Chem.* **2019**, *84*, 11343.

[43] A. Karton, *J. Phys. Chem. A* **2020**, *124*, 6977.

[44] A. A. Kroeger, A. Karton, *Chem. Eur. J.* **2021**, *27*, 3420.

[45] J. P. Perdew, K. Burke, M. Ernzerhof, *Phys. Rev. Lett.* **1996**, *77*, 3865.

[46] A. D. Becke, *J. Chem. Phys.* **1993**, *98*, 5648.

[47] S. Grimme, S. Ehrlich, L. Goerigk, *J. Comput. Chem.* **2011**, *32*, 1456.

[48] F. Weigend, R. Ahlrichs, *Phys. Chem. Chem. Phys.* **2005**, *7*, 3297.

[49] S. Grimme, *WIREs Comput. Mol. Sci.* **2011**, *1*, 211.

[50] A. D. Becke, E. R. Johnson, *J. Chem. Phys.* **2005**, *123*, 154101.

[51] A. Karton, P. R. Spackman, *J. Comput. Chem.* **2021**, *42*, 1590.

[52] P. Morgante, R. Peverati, *Chem. Phys. Lett.* **2021**, *765*, 138281.

[53] É. Brémond, M. Savarese, N. Q. Su, Á. J. Pérez-Jiménez, X. Xu, J. C. Sancho-Garcia, C. Adamo, *J. Chem. Theory Comput.* **2016**, *12*, 459.

[54] M. Piccardo, E. Penocchio, C. Puzzarini, M. Biczysko, V. Barone, *J. Phys. Chem. A* **2015**, *119*, 2058.

[55] L. Simon, J. M. Goodman, *Org. Biomol. Chem.* **2011**, *9*, 689.

[56] C. Gonzalez, H. B. Schlegel, *J. Chem. Phys.* **1989**, *90*, 2154.

[57] Y. Zhao, D. G. Truhlar, *J. Phys. Chem. A* **2005**, *109*, 5656.

[58] E. Caldeweyher, C. Bannwarth, S. Grimme, *J. Chem. Phys.* **2017**, *147*, 34112.

[59] E. Caldeweyher, S. Ehlert, A. Hansen, H. Neugebauer, S. Spicher, C. Bannwarth, S. Grimme, *J. Chem. Phys.* **2019**, *150*, 154112.

[60] L. Goerigk, A. Hansen, C. Bauer, S. Ehrlich, A. Najibi, S. Grimme, *Phys. Chem. Chem. Phys.* **2017**, *19*, 32184.

[61] A. Karton, *J. Comput. Chem.* **2017**, *38*, 370.

[62] L. Goerigk, R. Sharma, *Can. J. Chem.* **2016**, *94*, 1133.

[63] A. Karton, L. Goerigk, *J. Comput. Chem.* **2015**, *36*, 622.

[64] L. Goerigk, S. Grimme, *Phys. Chem. Chem. Phys.* **2011**, *13*, 6670.

[65] A. Karton, D. Gruzman, J. M. L. Martin, *J. Phys. Chem. A* **2009**, *113*, 8434.

[66] J. Zheng, Y. Zhao, D. G. Truhlar, *J. Chem. Theory Comput.* **2009**, *5*, 808.

[67] A. Karton, A. Tarnopolsky, J.-F. Lamère, G. C. Schatz, J. M. L. Martin, *J. Phys. Chem. A* **2008**, *112*, 12868.

[68] M. J. Frisch, G. W. Trucks, H. B. Schlegel, G. E. Scuseria, M. A. Robb, J. R. Cheeseman, G. Scalmani, V. Barone, G. A. Petersson, H. Nakatsuji, X. Li, M. Caricato, A. V. Marenich, J. Bloino, B. G. Janesko, R. Gomperts, B. Mennucci, H. P. Hratchian, J. V. Ortiz, A. F. Izmaylov, J. L. Sonnenberg, D. Williams-Young, F. Ding, F. Lipparini, F. Egidi, J. Goings, B. Peng, A. Petrone, T. Henderson, D. Ranasinghe, V. G. Zakrzewski, J. Gao, N. Rega, G. Zheng, W. Liang, M. Hada, M. Ehara, K. Toyota, R. Fukuda, J. Hasegawa, M. Ishida, T. Nakajima, Y. Honda, O. Kitao, H. Nakai, T. Vreven, K. Throssell, J. A. Montgomery, J. E. Peralta, F. Ogliaro, M. J. Bearpark, J. J. Heyd, E. N. Brothers, K. N. Kudin, V. N. Staroverov, T. A. Keith, R. Kobayashi, J. Normand, K. Raghavachari, A. P. Rendell, J. C. Burant, S. S. Iyengar, J. Tomasi, M. Cossi, J. M. Millam, M. Klene, C. Adamo, R. Cammi, J. W. Ochterski, R. L. Martin, K. Morokuma, O. Farkas, J. B. Foresman, D. J. Fox, *Gaussian 16, Revision A.03*, Gaussian, Inc., Wallingford, CT **2016**.

[69] P. v. R. Schleyer, C. Maerker, A. Dransfeld, H. Jiao, N. J. R. van Eikema Hommes, *J. Am. Chem. Soc.* **1996**, *118*, 6317.

[70] Z. Chen, C. S. Wannere, C. Corminboeuf, R. Puchta, P. v. R. Schleyer, *Chem. Rev.* **2005**, *105*, 3842.

[71] A. Rahalkar, A. Stanger, "Aroma" package; https://chemistry.technion.ac.il/members/amnon-stanger/.

[72] A. Stanger, *J. Org. Chem.* **2006**, *71*, 883.

[73] R. Gershoni-Poranne, A. Stanger, *Chem. Soc. Rev.* **2015**, *44*, 6597.

[74] D. Geuenich, R. Herges, *J. Phys. Chem. A* **2001**, *105*, 3214.

[75] D. Geuenich, K. Hess, F. Koehler, R. Herges, *Chem. Rev.* **2005**, *105*, 3758.

[76] P. R. Horn, Y. Mao, M. Head-Gordon, *Phys. Chem. Chem. Phys.* **2016**, *18*, 23067.

[77] N. Mardirossian, M. Head-Gordon, *J. Chem. Phys.* **2016**, *144*, 214110.

[78] Y. H. Shao, Z. T. Gan, E. Epifanovsky, A. T. B. Gilbert, M. Wormit, J. Kussmann, A. W. Lange, A. Behn, J. Deng, X. T. Feng, D. Ghosh, M. Goldey, P. R. Horn, L. D. Jacobson, I. Kaliman, R. Z. Khaliullin, T. Kus, A. Landau, J. Liu, E. I. Proynov, Y. M. Rhee, R. M. Richard, M. A. Rohrdanz, R. P. Steele, E. J. Sundstrom, H. L. Woodcock, P. M. Zimmerman, D. Zuev, B. Albrecht, E. Alguire, B. Austin, G. J. O. Beran, Y. A. Bernard, E. Berquist, K. Brandhorst, K. B. Bravaya, S. T. Brown, D. Casanova, C. M. Chang, Y. Q. Chen, S. H. Chien, K. D. Closser, D. L. Crittenden, M. Diedenhofen, R. A. DiStasio, H. Do, A. D. Dutoi, R. G. Edgar, S. Fatehi, L. Fusti-Molnar, A. Ghysels, A. Golubeva-Zadorozhnaya, J. Gomes, M. W. D. Hanson-Heine, P. H. P. Harbach, A. W. Hauser, E. G. Hohenstein, Z. C. Holden, T. C. Jagau, H. J. Ji, B. Kaduk, K. Khistyaev, J. Kim, J. Kim, R. A. King, P. Klunzinger, D. Kosenkov, T. Kowalczyk, C. M. Krauter, K. U. Lao, A. D. Laurent, K. V. Lawler, S. V. Levchenko, C. Y. Lin, F. Liu, E. Livshits, R. C. Lochan, A. Luenser, P. Manohar, S. F. Manzer, S. P. Mao, N. Mardirossian, A. V. Marenich, S. A. Maurer, N. J. Mayhall, E. Neuscamman, C. M. Oana, R. Olivares-Amaya, D. P, J. A. Neill, T. M. Parkhill, R. Perrine, A. Peverati, D. R. Prociuk, E. Rehn, N. J. Rosta, S. M. Russ, S. Sharada, D. W. Sharma, A. Small, T. Sodt, D. Stein, Y. C. S. Stuck, A. J. W. Thom, T. Tsuchimochi, V. Vanovschi, L. Vogt, O. Vydrov, T. Wang, M. A. Watson, J. Wenzel, A. White, C. F.

Williams, J. Yang, S. Yeganeh, S. R. Yost, Z. Q. You, I. Y. Zhang, X. Zhang, Y. Zhao, B. R. Brooks, G. K. L. Chan, D. M. Chipman, C. J. Cramer, W. A. Goddard, M. S. Gordon, W. J. Hehre, A. Klamt, H. F. Schaefer, M. W. Schmidt, C. D. Sherrill, D. G. Truhlar, A. Warshel, X. Xu, A. Aspuru-Guzik, R. Baer, A. T. Bell, N. A. Besley, J. D. Chai, A. Dreuw, B. D. Dunietz, T. R. Furlani, S. R. Gwaltney, C. P. Hsu, Y. S. Jung, J. Kong, D. S. Lambrecht, W. Z. Liang, C. Ochsenfeld, V. A. Rassolov, L. V. Slipchenko, J. E. Subotnik, T. Van Voorhis, J. M. Herbert, A. I. Krylov, P. M. W. Gill, M. Head-Gordon, *Mol. Phys.* **2015**, *113*, 184.

[79] C. F. Macrae, I. Sovago, S. J. Cottrell, P. T. A. Galek, P. McCabe, E. Pidcock, M. Platings, G. P. Shields, J. S. Stevens, M. Towler, P. A. Wood, *J. Appl. Crystallogr.* **2020**, *53*, 226.

[80] C. Y. Legault, CYLview, 1.0b, Universite de Sherbrooke, **2009**, http://www.cylview.org.

[81] S. K. Dominique, S. Lobsiger, H. M. Frey, S. Leutwyler, J. F. Stanton, *J. Phys. Chem. A* **2008**, *112*, 9134.

[82] J. Bordner, R. H. Stanford, R. G. Parker, *Acta Crystallogr., Sect. B: Struct. Crystallogr. Cryst. Chem.* **1972**, *28*, 1069.

[83] K. H. Claus, C. Krüger, *Acta Crystallogr.* **1988**, *C44*, 1632.

[84] A. Karton, J. M. L. Martin, *J. Chem. Phys.* **2012**, *136*, 124114.

[85] A. Karton, *WIREs Comput. Mol. Sci.* **2016**, *6*, 292.

[86] J. L. Marshall, K. Uchida, C. K. Frederickson, C. Schütt, A. M. Zeidell, K. P. Goetz, T. W. Finn, K. Jarolimek, L. N. Zakharov, C. Risko, R. Herges, O. D. Jurchescu, M. M. Haley, *Chem. Sci.* **2016**, *7*, 5547.

[87] R. Gershoni-Poranne, A. Stanger, *Chem. Eur. J.* **2014**, *20*, 5673.

[88] We cannot exclude the possibility that the planar catalyzed TSs also exist, however, despite numerous attempts, we were not able to locate the tub-inversion TSs of DBCOT and DNCOT on graphene, i.e., the planar structures always converge to local minima.

[89] Y. Zhao, D. G. Truhlar, *Theor. Chem. Acc.* **2008**, *120*, 215.

[90] Y. Zhao, D. G. Truhlar, *Chem. Phys. Lett.* **2011**, *502*, 1.

[91] C. J. Cramer, *Essentials of Computational Chemistry: Theories and Models*, Wiley, Hoboken **2004**.

[92] M. D. Halls, H. Bernhard Schlegel, *J. Phys. Chem.* **1921**, *B2002*, 106.

[93] P. Giacinto, F. Zerbetto, A. Bottoni, M. Calvaresi, *J. Chem. Theory Comput.* **2016**, *12*, 4082.

[94] I. S. Tavares, C. F. B. R. Figueiredo, A. L. Magalhães, *J. Phys. Chem. C* **2017**, *121*, 2165.

[95] I. Alves, A. L. Magalhães, *J. Phys. Chem. A* **2019**, *123*, 8188.

[96] W. Zheng, S. A. Yamada, S. T. Hung, W. Sun, L. Zhao, M. D. Fayer, *J. Am. Chem. Soc.* **2020**, *142*, 5636.

[97] A. Karton, R. J. O'Reilly, D. I. Pattison, M. J. Davies, L. Radom, *J. Am. Chem. Soc.* **2012**, *134*, 19240.

[98] E. Solel, D. Pappo, O. Reany, T. Mejuch, R. Gershoni-Poranne, M. Botoshansky, A. Stanger, E. Keinan, *Chem. Sci.* **2020**, *11*, 13015.

[99] I. B. Bersuker, *Chem. Rev.* **2021**, *121*, 1463.

[100] I. B. Bersuker, *Symmetry* **2021**, *13*, 1577.

[101] I. B. Bersuker, *FlatChem.* **2017**, *6*, 11.

[102] N. Gorinchoy, *Int. J. Org. Chem.* **2018**, *08*, 142.

[103] N. N. Gorinchoy, I. B. Bersuker, *J. Phys.: Conf. Ser.* **2017**, *833*, 012010.

[104] S. Grimme, *Angew. Chem., Int. Ed.* **2008**, *47*, 3430.

[105] J. Cioslowski, *J. Am. Chem. Soc.* **1989**, *111*, 8333.

[106] F. De Proft, J. M. L. Martin, P. Geerlings, *Chem. Phys. Lett.* **1996**, *250*, 393.

[107] M. Cho, N. Sylvetsky, S. Eshafi, G. Santra, I. Efremenko, J. M. L. Martin, *Chem. Phys. Chem.* **2020**, *21*, 688.

SUPPORTING INFORMATION

Additional supporting information may be found in the online version of the article at the publisher's website.